

Oscillation of Dzyaloshinskii-Moriya interaction driven by weak electric fields

Runze Chen(陈润泽), Anni Cao(曹安妮), Xinran Wang(王馨苒), Yang Liu(柳洋), Hongxin Yang(杨洪新), and Weisheng Zhao(赵巍胜)

Citation: Chin. Phys. B, 2024, 33 (**2**): 027501. DOI: 10.1088/1674-1056/ad0f85
Journal homepage: http://cpb.iphy.ac.cn; http://iopscience.iop.org/cpb

What follows is a list of articles you may be interested in

Influence of Dzyaloshinskii-Moriya interaction on the magnetic vortex reversal in an off-centered nanocontact geometry

Hua-Nan Li(李化南), Tong-Xin Xue(薛彤鑫), Lei Chen(陈磊), Ying-Rui Sui(隋瑛瑞), and Mao-Bin Wei(魏茂彬)†
Chin. Phys. B, 2022, 31 (**9**): 097501. DOI: 10.1088/1674-1056/ac4cbd

Synchronization of nanowire-based spin Hall nano-oscillators

Biao Jiang(姜彪), Wen-Jun Zhang(张文君), Mehran Khan Alam, Shu-Yun Yu(于淑云), Guang-Bing Han(韩广兵), Guo-Lei Liu(刘国磊), Shi-Shen Yan(颜世申), and Shi-Shou Kang(康仕寿)
Chin. Phys. B, 2022, 31 (**7**): 077503. DOI: 10.1088/1674-1056/ac560a

Exact soliton solutions in anisotropic ferromagnetic wires with Dzyaloshinskii-Moriya interaction

Qiu-Yan Li(李秋艳), Dun-Zhao(赵敦), and Zai-Dong Li(李再东)
Chin. Phys. B, 2021, 30 (**1**): 017504. DOI: 10.1088/1674-1056/abca26

Spin waves and transverse domain walls driven by spin waves: Role of damping

Zi-Xiang Zhao(赵梓翔), Peng-Bin He(贺鹏斌), Meng-Qiu Cai(蔡孟秋), Zai-Dong Li(李再东)
Chin. Phys. B, 2020, 29 (**7**): 077502. DOI: 10.1088/1674-1056/ab90e5

Realization of artificial skyrmion in CoCrPt/NiFe bilayers

Yi Liu(刘益), Yong-Ming Luo(骆泳铭), Zheng-Hong Qian(钱正洪), Jian-Guo Zhu(朱建国)
Chin. Phys. B, 2018, 27 (**12**): 127503. DOI: 10.1088/1674-1056/27/12/127503

Oscillation of Dzyaloshinskii–Moriya interaction driven by weak electric fields

Runze Chen(陈润泽)[1], Anni Cao(曹安妮)[5], Xinran Wang(王馨苒)[1,3], Yang Liu(柳洋)[1], Hongxin Yang(杨洪新)[4], and Weisheng Zhao(赵巍胜)[1,2,3,†]

[1] *Fert Beijing Institute, MIIT Key Laboratory of Spintronics, School of Integrated Circuit Science and Engineering, Beihang University, Beijing* 100191, *China*

[2] *Hefei Innovation Research Institute, Beihang University, Hefei* 230013, *China*

[3] *Beihang-Goertek Joint Microelectronics Institute, Qingdao Research Institute, Beihang University, Qingdao* 266000, *China*

[4] *National Laboratory of Solid State Microstructures, School of Physics, Collaborative Innovation Center of Advanced Microstructures, Nanjing University, Nanjing* 210093, *China*

[5] *Beijing Microelectronics Technology Institute, Beijing* 100076, *China*

(Received 13 September 2023; revised manuscript received 13 November 2023; accepted manuscript online 24 November 2023)

Dzyaloshinskii–Moriya interaction (DMI) is under extensive investigation considering its crucial status in chiral magnetic orders, such as Néel-type domain wall (DW) and skyrmions. It has been reported that the interfacial DMI originating from Rashba spin–orbit coupling (SOC) can be linearly tuned with strong external electric fields. In this work, we experimentally demonstrate that the strength of DMI exhibits rapid fluctuations, ranging from 10% to 30% of its original value, as a function of applied electric fields in Pt/Co/MgO heterostructures within the small field regime ($< 10^{-2}$ V/nm). Brillouin light scattering (BLS) experiments have been performed to measure DMI, and first-principles calculations show agreement with this observation, which can be explained by the variation in orbital hybridization at the Co/MgO interface in response to the weak electric fields. Our results on voltage control of DMI (VCDMI) suggest that research related to the voltage control of magnetic anisotropy for spin–orbit torque or the motion control of skyrmions might also have to consider the role of the external electric field on DMI as small voltages are generally used for the magnetoresistance detection.

Keywords: Dzyaloshinskii–Moriya interaction, weak electric field control effect, Rashba spin–orbit coupling, interfacial orbital hybridization

PACS: 75.47.–m, 85.75.–d, 71.70.Ej **DOI:** 10.1088/1674-1056/ad0f85

1. Introduction

In recent years, with the booming development of spintronic devices, more efficient methods are required to improve storage density, reduce power consumption, and enhance stability.[1–3] It has been realized that voltage-controlled magnetic anisotropy (VCMA) combing with spin–orbit torque (SOT) can be a promising manipulation to decrease the critical switching current for both in-plane and perpendicularly magnetized magnetic tunnel junctions (MTJs) in magnetic random-access memory (MRAM).[4–6] Similarly, with the assistance of the electric (E) field, the domain wall (DW) motion in race-track devices could also be improved.[7] Electrical control of magnetism seems to have great potential for various spintronic applications. Dzyaloshinskii–Moriya interaction (DMI), as one of the key ingredients for magnetic skyrmions and chiral domain walls (DWs),[8–13] arises from the presence of spin–orbit coupling (SOC) and inversion symmetry breaking system. Recent studies suggest that the Rashba effect, which is sensitive to the interfacial potential, can contribute to the DMI at the ferromagnet/oxide interface, thereby providing the possibility of external E-field control over DMI.[14–16] Pieces of experimental evidence have been reported that the DMI energy can be linearly changed in Ta/FeCoB/TaO_x stacks[17] and in MgO/Fe/Pt multilayers by hundreds of volts gate-voltage.[18] Meanwhile, groups of research on the dynamics of skyrmion controlled through gate-voltage have been demonstrated[19–21] and were suggested to be of relevance in the field of neuromorphic computing[22,23] as well as electrical logic devices.[24] However, the general trend of DMI energy over electric field remains elusive, especially for weak E-field, which is closely related to the magnetoresistance detection and electronic device applications. Without a thorough understanding of VCDMI, further applications of electric field on the system of skyrmion, STT, and SOT would be incomplete and doubtful.

In this paper, we carried out BLS measurements on Pt/Co/MgO samples applied with electric field from 10^{-5} V/nm to 10^{-2} V/nm. The trends of DMI energy were observed fluctuating about 15%–30% of its original value with a weak E-field. To confirm the experimental results, we obtained the theoretical DMI strength through *ab initio* calculations and achieved results consistent with experimental observations, particularly in response to the weak voltage-induced DMI fluctuations. Moreover, based on the Rashba model, we explained the behavior of DMI under the weak voltage through

[†]Corresponding author. E-mail: weisheng.zhao@buaa.edu.cn

© 2024 Chinese Physical Society and IOP Publishing Ltd

calculations of the Rashba SOC energy source and the corresponding SOC orbital hybridization matrix at the Co/MgO interface.

2. Results and discussion

By using magnetron sputtering at room temperature, we grow Ta(3 nm)/Pt(4 nm)/Co(t_{Co})/MgO(2 nm)/SiO_2(5 nm) samples shown as in Fig. 1(a), with t_{Co} varying from 1.5 nm to 2.3 nm. The base pressure of our ultrahigh vacuum deposition system is around 3×10^{-8} mbar (1 bar = 10^5 Pa). The substrates we use are silicon plates with 100-nm thermal silicon oxide layers. It has been proved in our previous studies[25,26] that an inserted dusting layer between Co and MgO can prevent the deterioration of the Co/MgO interface during the deposition process, thus we also use Ta and W, as a 0.2-nm inserted layer X between Co and MgO, to improve the crystallization for both ferromagnetic and insulating layers. The top SiO_2 layer prevents the film from air-passivation. After the deposition, the thin films were fabricated into 2-mm stripes with perpendicular top electrodes, as we introduced in supporting information part I.

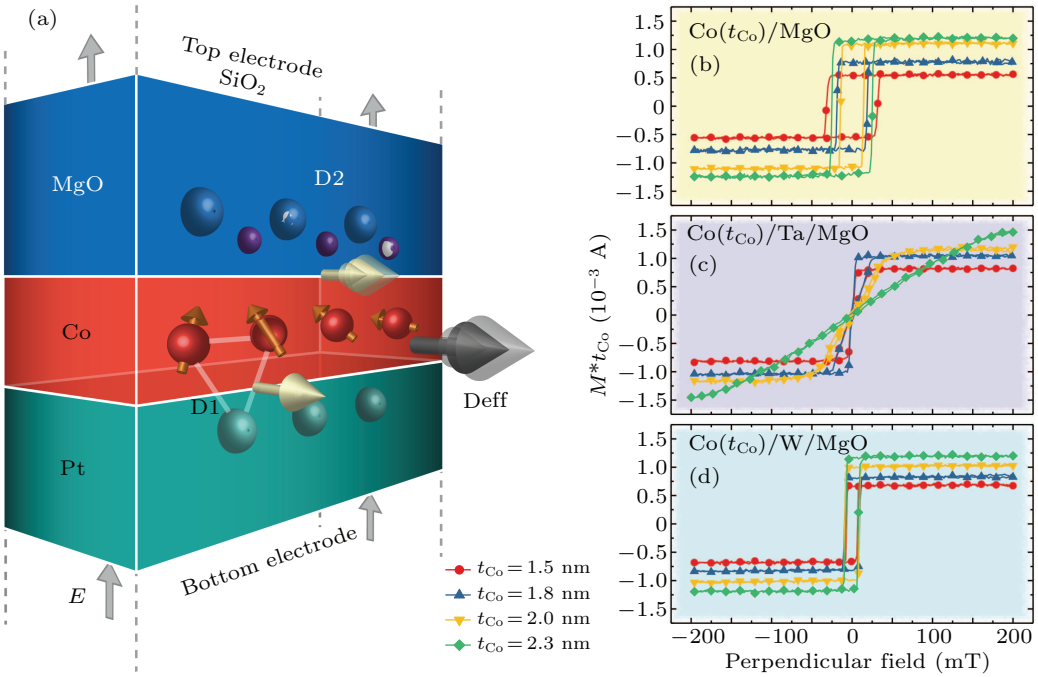


Fig. 1. (a) An illustration of VCDMI in Pt/Co/MgO system. Hysteresis loops with perpendicular magnetic field for (b) Pt/Co(t_{Co})/MgO, (c) Pt/Co(t_{Co})/Ta/MgO, and (d) Pt/Co(t_{Co})/W/MgO.

We measured the hysteresis loops of our samples using a vibrating sample magnetometer (VSM). As shown in Figs. 1(b)–1(d), except for Pt/Co(2.0 nm and 2.3 nm)/Ta/MgO, all the other samples exhibit clear perpendicular magnetic anisotropy (PMA). Loops with the in-plane field can be found in supporting information part II. By comparing the same color (same t_{Co}) loops shown in Figs. 1(b)–1(d), we found that samples without an inserted layer exhibit almost the smallest saturated moment, while the largest saturated moment appears in samples inserted by Ta, indicating the thinnest magnetic dead layer t_{dead} with the same Co thickness. All of the structures were annealed for half an hour at 300 °C and 350 °C. We analyzed the magnetic properties and dead layer of these samples in supporting information part III.

We quantified the strength of DMI for our sample employing a BLS set-up. It is ideally suited for studying the DMI of Pt/FM multilayers thanks to its sub-GHz resolution and few nm surface sensitivity.[27] As shown in Fig. 2(a), taking Pt/Co(1.5)/Ta/MgO as an example, when the angle between incident light and interface normal $\theta = 50°$, after fitting the Stokes and anti-Stokes signals by Lorentzian function, the frequency difference Δf can be obtained. By varying the angle θ of the incident light, we have results of different wave vectors k according to $k = 4\pi\sin(\theta)/\lambda$,[28–30] as shown in Fig. 2(b). Here λ is the wavelength of the incident light. Furthermore, the DMI energy can be obtained by $\Delta f = (2\gamma D/\pi M_s)k$.[31,32] By taking $\gamma/2\pi = 31$ GHz/T[33] and M_s measured by VSM into this equation, the DMI energy D can be calculated. Note that the chirality of our Pt/Co/MgO system is inverted with respect to Ta/CoFeB/MgO in which the D value measured by BLS is positive.[28] The results of D for samples in different annealing states can be found in supporting information part IV.

We applied E-fields ranging from 10^{-5} V/nm–10^{-2} V/nm on our devices and measured the DMI energy D by the method introduced above. A selection of results is shown in Figs. 2(c)–2(f). At higher electric field ($\geq 10^{-2}$ V/nm), we find linear trends with a slope of typically -0.2 mJ/m^2 per V/nm. How-

ever, much more surprisingly, we find that the DMI energies oscillate at a low electric field ($< 10^{-2}$ V/nm). For samples with different t_{Co} as well as inserted layers, the amplitude of the oscillations varies by 0.1 mJ/m^2 to 0.2 mJ/m^2, corresponding to 14% to 29% of its original value. All of the samples exhibit such vibration part of D, which could prove the generality of this phenomenon.

First-principles calculations are employed to confirm and explain the trends of D over the E-field. The crystalline structure of the MgO(3 monolayers)/Co(3 monolayers)/Pt(3 monolayers) is illustrated in Fig. 3(a), with the MgO surface passivated by hydrogen at the bottom side, and a 15-Å vacuum layer on the top side. We applied the electric field along the z ([001]) direction from insulator to heavy metal by placing a dipole layer in the middle of the vacuum region.[34] More details about the calculation are introduced in supporting information part V. Note that we adopt a positive DMI representing CW (right-handed) chirality and a negative DMI representing ACW (left-handed) chirality. The microscopic DMI strength d^{tot} and micromagnetic DMI coefficient D^{tot} as a function of the E_{MgO} are presented in Fig. 3(b). E_{MgO} indicates the actual potential difference over the oxide layer. In the absence of an electric field, the interfacial microscopic DMI strength d^{tot} of the structure is −5.03 meV corresponding to the micromagnetic DMI coefficient D^{tot} of −7.24 mJ/m^2, which is consistent with the results reported in Ref. [35]. Following, we found a strong oscillation of DMI in the MgO/Co/Pt structure relative to the electric field within the range of a small scale. However, when we increase the order of the electric field, the DMI of the structure varies linearly with the electric field, as shown in Fig. 3(b). When a positive (negative) electric field is applied, the absolute value of DMI energy increases (decreases), which is consistent with both the experimental and the calculation results reported by others.[35,36] The trend of DMI we obtained from *ab initio* calculations agrees well with our experimental results.

To gain an insight into the origin of the trend of the DMI magnitude relative to the electric field, we plot the potential difference at the MgO/Co interface ΔE_{MgO-Co} and the Co/Pt interface ΔE_{Co-Pt} as a function of the electric field E_{MgO}, respectively, as shown in Fig. S7 in supporting information part V. We observed that as the external electric field varies, the potential difference at the MgO/Co interface shows alterations, while that at the Co/Pt interface remains nearly constant. This highlights the MgO/Co interface as the primary factor shaping the behavior of VCDMI, directing our further analysis toward understanding its pivotal role.

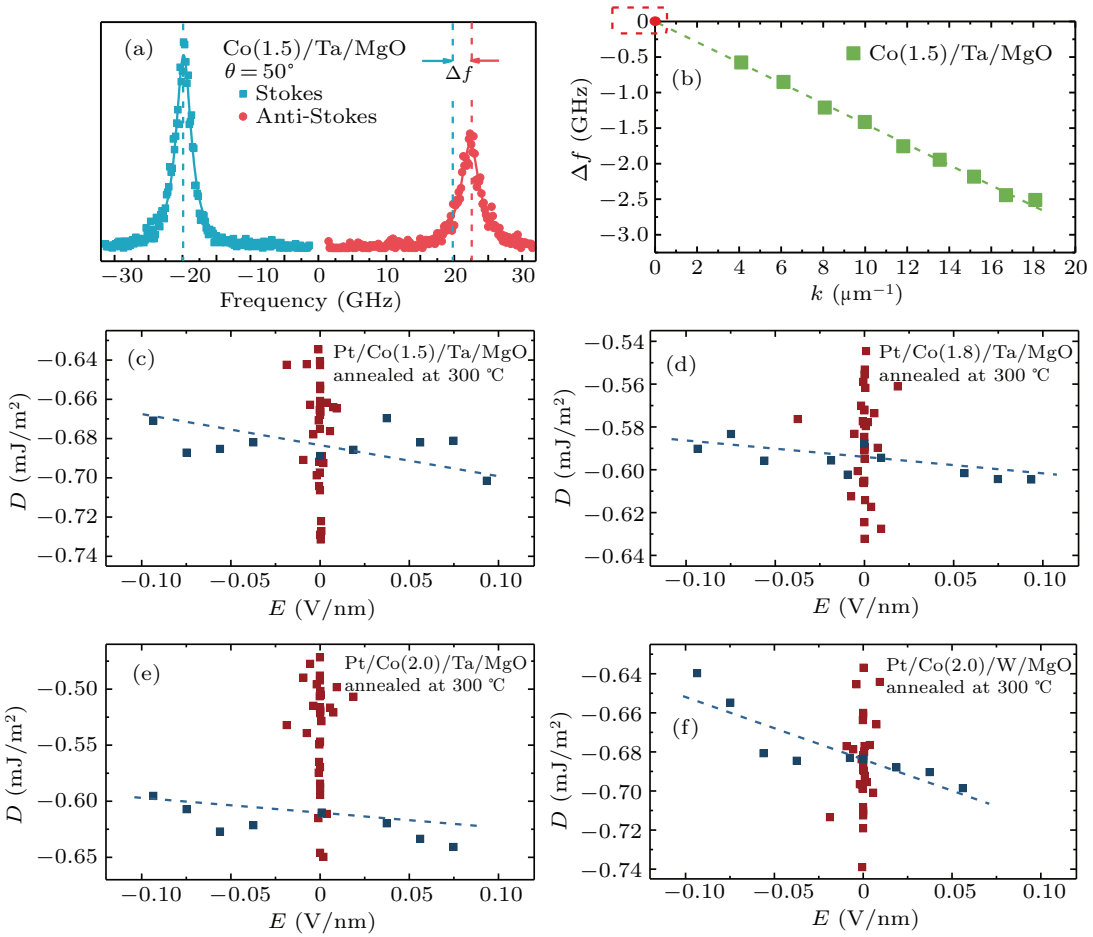


Fig. 2. (a) BLS spectra for spin waves of DE mode. (b) The linear dependence of Δf on k. Experimental results of voltage-influenced DMI for (c) Pt/Co(1.5)/Ta/MgO, (d) Pt/Co(1.8)/Ta/MgO, (e) Pt/Co(2.0)/Ta/MgO, and (f) Pt/Co(2.0)/W/MgO annealed at 300 °C.

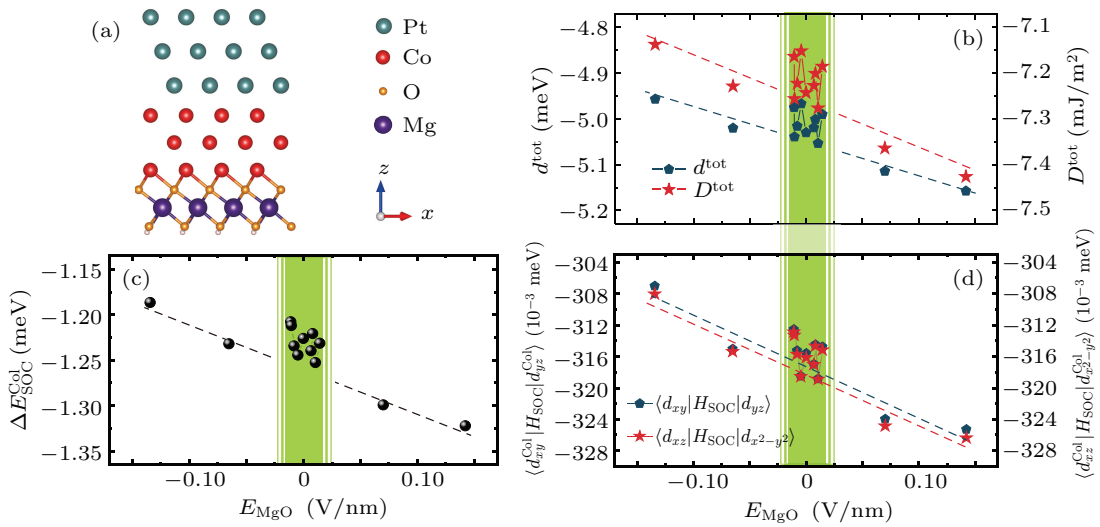


Fig. 3. (a) The ideal array of atoms of Pt/Co/MgO structure used for the first-principles calculations. (b) The calculated total DMI strength $d^{\rm tot}$ and micro-magnetic DMI energy $D^{\rm tot}$ vary with the electric field. (c) The trend of Rashba SOC energy source at MgO/Co interface $\Delta E_{\rm SOC}^{\rm Co1}$ with the electric field. (d) The trend of SOC orbital hybridization terms in interfacial Co layer $\langle d_{xy}^{\rm Co1}|H_{\rm SOC}|d_{yz}^{\rm Co1}\rangle$ and $\langle d_{xz}^{\rm Co1}|H_{\rm SOC}|d_{x^2-y^2}^{\rm Co1}\rangle$ with the electric field.

Recent theoretical studies have suggested that the Rashba spin–orbit coupling (SOC) at the interface between a ferromagnet and an oxide can lead to Rashba-type DMI, which can be explained through the Rashba effect.[35,37,38] Therefore, we can further analyze the origin of the trend of VCDMI at the MgO/Co interface by utilizing the formalism of Rashba SOC. We calculated the layer-resolved SOC energy distribution for the MgO/Co/Pt structure in the absence of an external electric field, as illustrated in Fig. S8 in supporting information part V. It is evident that the SOC energy source for DMI at the MgO/Co interface is predominately located within the interfacial Co1 layer. This indicates the pivotal role played by the SOC energy difference of interfacial Co1 layer $\Delta E_{\rm SOC}^{\rm Co1}$ in determining the DMI energy of the MgO/Co interface, which aligns with the significant characteristic of DMI induced by the Rashba effect.[15,35,39]

Furthermore, the trend of the Rashba SOC energy source at the MgO/Co interface $\Delta E_{\rm SOC}^{\rm Co1}$ with the E-field was calculated, as depicted in Fig. 3(c). We observed a variation trend consistent with VCDMI. Specifically, $\Delta E_{\rm SOC}^{\rm Co1}$ exhibits pronounced fluctuations within the small range of electric field values, while at higher voltage levels, the Rashba SOC energy source shows a linear relationship with the electric field. Thus, the modulation trend of DMI energy with the electric field originates from the variation behavior of the Rashba SOC energy in the interfacial Co layer in response to the voltage.

It has been reported that, within the Rashba SOC formalism, alternations in the degree of orbital hybridization can effectively tune DMI in systems with broken spatial inversion symmetry. This can be achieved through modification of the electric interface dipole by the absorption of electronegative ions at the surface, such as oxygen or hydrogen atoms,[39,40] thereby tuning the interfacial atomic orbitals. Essentially, these modifications stem from the intimate relationship between DMI and the interfacial orbital hybridization caused by SOC, which can be described by the SOC orbital hybridization matrix.[41–43] To further elucidate the origin of the variation behavior of the Rashba SOC energy in the interfacial Co layer, we initially calculated the 3d orbital-resolved SOC energy of the interfacial Co atoms at zero voltage, as shown in Fig. S9 in supporting information part V. It can be observed that the strongest contribution to DMI comes from the SOC matrix elements corresponding to the orbital hybridization between d_{xy} and d_{yz}, as well as d_{xz} and $d_{x^2-y^2}$ (red bars), which can be denoted in the form of expectation values $\langle d_{xy}^{\rm Co1}|H_{\rm SOC}|d_{yz}^{\rm Co1}\rangle$ and $\langle d_{xz}^{\rm Co1}|H_{\rm SOC}|d_{x^2-y^2}^{\rm Co1}\rangle$, respectively. Subsequently, we investigated the trends of these two SOC orbital hybridization terms with the electric field. We observed that both orbital terms undergo significant oscillations within a narrow voltage range. However, as the E-field varies in a wide range, they demonstrate a linear response to the applied E-field, as depicted in Fig. 3(d). To sum up, it is the variation behavior of specific SOC orbital hybridization terms in the interfacial Co layer with external E-field that results in a comparable trend in the Rashba SOC energy source at the MgO/Co interface, ultimately manifesting as a voltage-control behavior of DMI.

3. Conclusion

In conclusion, we experimentally found a considerable oscillation of DMI with a weak electrical field in a series of samples, and theoretically confirmed the trend through *ab initio* calculation. The variation in the Rashba SOC energy source at the MgO/Co interface, more fundamentally, the change of the degree of SOC orbital hybridization at the interface is responsible for the fluctuation of DMI with the weak electric field, which is often neglected in most research. Hence, the surprising behavior of VCDMI we found refreshes

the traditional perception of modulation by an electrical field and processes the guiding significance for studies on voltage control of skyrmion's motion as well as the STT and SOT systems assisted by VCMA.

Supplementary material

See the supplementary material for details on fabrication of device, in-plane hysteresis loops, analysis of magnetic properties, DMI strength of samples in different states, and first-principles calculations.

Acknowledgements

Project supported by the National Natural Science Foundation of China (Grant Nos. 61627813, 62204018, and 61571023), the Beijing Municipal Science and Technology Project (Grant No. Z201100004220002), the National Key Technology Program of China (Grant No. 2017ZX01032101), the Program of Introducing Talents of Discipline to Universities in China (Grant No. B16001), and the VR Innovation Platform from Qingdao Science and Technology Commission.

References

[1] Du A, Zhu D Q, Cao K H, Zhang Z Z, Guo Z X, Shi K W, Xiong D R, Xiao R, Cai W L, Yin J L, Lu S Y, Zhang C, Zhang Y, Luo S J, Fert A and Zhao W S 2023 *Nat. Electron.* **6** 425

[2] Peng S Z, Zhu D Q, Li W X, Wu H, Grutter A J, Gilbert D A, Lu J Q, Xiong D R, Cai W L, Shafer P, Wang K L and Zhao W S 2020 *Nat. Electron.* **3** 757

[3] Wang L D, Cheng H Y, Li P Z, Hees Y L W, Liu Y, Cao K H, Lavrijsen R, Lin X Y, Koopmans B and Zhao W S 2022 *Proc. Natl. Acad. Sci. USA* **119** e2204732119

[4] Yoda H, Shimomura N, Ohsawa Y, Shirotori S, Kato Y, Inokuchi T, Kamiguchi Y, Altansargai B, Saito Y, Koi K, Sugiyama H, Oikawa S, Shimizu M, Ishikawa M, Ikegami K and Kurobe A 2016 *IEEE International Electron Devices Meeting (IEDM)*, December 3–7, 2016, San Francisco, CA, USA, p. 27.6.1

[5] Peng S Z, Lu J Q, Li W X, Wang L Z, Zhang H, Li X, Wang K L and Zhao W S 2019 *IEEE International Electron Devices Meeting (IEDM)*, December 7–11, 2019, San Francisco, CA, USA, p. 28.6.1

[6] Guo Z X, Yin J L, Bai Y, Zhu D Q, Shi K W, Wang G F, Cao K H and Zhao W S 2021 *Proc. IEEE* **109** 1398

[7] Parkin S S P, Hayashi M and Thomas L 2008 *Science* **320** 190

[8] Fert A, Reyren N and Cros V 2017 *Nat. Rev. Mater.* **2** 17031

[9] Li S, Du A, Wang Y D, Wang X R, Zhang X Y, Cheng H Y, Cai W L, Lu S Y, Cao K H, Pan B, Lei N, Kang W, Liu J M, Fert A, Hou Z P and Zhao W S 2022 *Sci. Bull.* **67** 691

[10] Cui Q R, Liang J H, Zhu Y M, Yao X and Yang H X 2023 *Chin. Phys. Lett.* **40** 037502

[11] Li H N, Xue T X, Chen L, Sui Y R and Wei M B 2022 *Chin. Phys. B* **31** 097501

[12] Li K K 2023 *Chin. Phys. Lett.* **40** 027502

[13] Wang XR, Cao A N, Li S, Tang J, Du A, Cheng H Y, Sun Y M, Du H F, Zhang X Y and Zhao W S 2021 *Phys. Rev. B* **104** 064421

[14] Kim K W, Lee H W, Lee K J and Stiles M D 2013 *Phys. Rev. Lett.* **111** 216601

[15] Yang H X, Chen G, Cotta A A C, N'Diaye A T, Nikolaev S A, Soares E A, Macedo W A A, Liu K, Schmid A K, Fert A and Chshiev M 2018 *Nat. Mater.* **17** 605

[16] Kundu A and Zhang S 2015 *Phys. Rev. B* **92** 094434

[17] Srivastava T, Schott M, Juge R, Křižáková V, Belmeguenai M, Roussigné Y, Bernand-Mantel A, Ranno L, Pizzini S, Chérif S M, Stashkevich A, Auffret S, Boulle O, Gaudin G, Chshiev M, Baraduc C and Béa H 2018 *Nano Lett.* **18** 4871

[18] Zhang W, Zhong H, Zang R, Zhang Y, Yu S, Han G, Liu G L, Yan S S, Kang S and Mei L M 2018 *Appl. Phys. Lett.* **113** 122406

[19] Schott M, Bernand-Mantel A, Ranno L, Pizzini S, Vogel J, Béa H, Baraduc C, Auffret S, Gaudin G and Givord D 2017 *Nano Lett.* **17** 3006

[20] Hsu P J, Kubetzka A, Finco A, Romming N, Bergmann K V and Wiesendanger R 2017 *Nat. Nanotechnol.* **12** 123

[21] Nozaki T, Jibiki Y, Goto M, Tamura E, Nozaki T, Kubota H, Fukushima A, Yuasa S and Suzuki Y 2019 *Appl. Phys. Lett.* **114** 012402

[22] Yu Z Y, Shen M K, Zeng Z M, Liang S H, Liu Y, Chen M, Zhang Z H, Lu Z H, You L, Yang X F, Zhang Y and Xiong R 2020 *Nanoscale Adv.* **2** 1309

[23] Luo S J, Xu N, Guo Z, Zhang Y, Hong J and You L 2019 *IEEE Electron Dev. Lett.* **40** 635

[24] Zhang Z Z, Zhu Y Z, Zhang Y, Zhang K, Nan J, Zheng Z Y, Zhang Y G and Zhao W S 2019 *IEEE Electron Dev. Lett.* **40** 1984

[25] Cao A N, Zhang X Y, Koopmans B, Peng S Z, Zhang Y, Wang Z L, Yan S H, Yang H X and Zhao W S 2018 *Nanoscale* **10** 12062

[26] Cao A N, Chen R Z, Wang X R, Zhang X Y, Lu S Y, Yan S S, Koopmans B and Zhao W S 2020 *Nanotechnology* **31** 155705

[27] Nembach H T, Shaw J M, Weiler M, Jué E and Silva T J 2015 *Nat. Phys.* **11** 825

[28] Ma X, Yu G Q, Li X, Wang T, Wu D, Olsson K S, Chu Z D, An K, Xiao J Q, Wang K L and Li X Q 2016 *Phys. Rev. B* **94** 180408

[29] Wang Z K, Zhang V L, Lim H S, Ng S C, Kuok M H, Jain S and Adeyeye A O 2009 *Appl. Phys. Lett.* **94** 083112

[30] Ma X, Yu G Q, Tang C, Li X, He C L, Shi J, Wang K L and Li X Q 2018 *Phys. Rev. Lett.* **120** 157204

[31] Di K, Zhang V L, Lim H S, Ng S C, Kuok M H, Qiu X P and Yang H 2015 *Appl. Phys. Lett.* **106** 052403

[32] Belmeguenai M, Adam J P, Roussigné Y, Eimer S, Devolder T, Kim J V, Cherif S M, Stashkevich A and Thiaville A 2015 *Phys. Rev. B* **91** 180405

[33] Belmeguenai M, Roussigne Y, Cherif S M, Stashkevich A, Petrisor J T, Nasui M and Gabor M S 2019 *J. Phys. D: Appl. Phys.* **52** 125002

[34] Neugebauer J and Matthias S 1992 *Phys. Rev. B* **46** 16067

[35] Yang H X, Boulle O, Cros V, Fert A and Chshiev M 2018 *Sci. Rep.* **8** 12356

[36] Suwardy J, Goto M, Suzuki Y and Miwa S 2019 *Jpn. J. Appl. Phys.* **58** 060917

[37] Manchon A, Koo H C, Nitta J, Frolov S M and Duine R A 2015 *Nat. Mater.* **14** 871

[38] Kikuchi T, Koretsune T, Arita R and Tatara G 2016 *Phys. Rev. Lett.* **116** 247201

[39] Yang B S, Cui Q R, Liang J H, Chshiev M and Yang H X 2020 *Phys. Rev. B* **101** 014406

[40] Belabbes A, Bihlmayer G, Blügel S and Manchon A 2016 *Sci. Rep.* **6** 24634

[41] Kashid V, Schena T, Zimmermann B, Mokrousov Y, Blügel S, Shah V and Salunke H G 2014 *Phys. Rev. B* **90** 054412

[42] Chen R Z, Wang X R, Cheng H Y, Lee K J, Xiong D R, Kim J Y, Li S, Yang H X, Zhang H C, Cao K H, Kläui M, Peng S Z, Zhang X Y and Zhao W S 2021 *Cell Rep. Phys. Sci.* **2** 100618

[43] Jadaun P, Register L F and Banerjee S K 2020 *npj Comput. Mater.* **6** 88